Tudisco et al. Nanoscale Research Letters (2018) 13:45
DOI 10.1186/s11671-018-2459-8

Nanoscale Research Letters

NANO EXPRESS

Open Access

Comparison Between Folic Acid and gH625 Peptide-Based Functionalization of Fe_3O_4 Magnetic Nanoparticles for Enhanced Cell Internalization

C. Tudisco[1,2†], M. T. Cambria[3†], A. E. Giuffrida[1,2], F. Sinatra[3], C. D. Anfuso[3], G. Lupo[3], N. Caporarello[3], A. Falanga[4], S. Galdiero[4], V. Oliveri[1], C. Satriano[1] and G. G. Condorelli[1,2*]

Abstract

A versatile synthetic route based on magnetic Fe_3O_4 nanoparticle (MNP) prefunctionalization with a phosphonic acid monolayer has been used to covalently bind the gH625 peptide on the nanoparticle surface. gH625 is a membranotropic peptide capable of easily crossing the membranes of various cells including the typical human blood-brain barrier components. A similar synthetic route was used to prepare another class of MNPs having a functional coating based on PEG, rhodamine, and folic acid, a well-known target molecule, to compare the performance of the two cell-penetrating systems (i.e., gH625 and folic acid). Our results demonstrate that the uptake of gH625-decorated MNPs in immortalized human brain microvascular endothelial cells after 24 h is more evident compared to folic acid-functionalized MNPs as evidenced by confocal laser scanning microscopy. On the other hand, both functionalized systems proved capable of being internalized in a brain tumor cell line (i.e., glioblastoma A-172). These findings indicate that the functionalization of MNPs with gH625 improves their endothelial cell internalization, suggesting a viable strategy in designing functional nanostructures capable of first crossing the BBB and, then, of reaching specific tumor brain cells.

Background

The blood-brain barrier (BBB) is a dynamic interface between the blood and the brain which plays a crucial role in the maintenance of the central nervous system (CNS) homeostasis. The main components of the BBB are the endothelial cells (i.e., astrocytes and pericytes), which form a continuous sheet covering the inner surface of the brain's microvessels. They are interconnected by tight junctions, which are critical to both the control of BBB vascular permeability [1] and to the protection of the brain from various circulating toxins and other harmful molecules [2, 3]. Neurons and microglia, which are other neurovascular unit components, play a different role in the BBB [4, 5].

Due to the endothelial cell continuous sheet, 98% of small-molecule drugs and 100% of large-molecule drugs do not pass through the BBB, thus failing to deliver the drugs to the brain tissue [6]. Therefore, in order to develop efficient delivery systems for the treatment of many brain diseases, it is crucial to investigate the carriers' ability of getting through the BBB [7].

In the last decade, nanoparticle-based systems have been widely studied as effective therapeutic agents for cancer targeting and therapy. In this context, organic functionalized magnetic iron nanoparticles (MNPs) have drawn a lot of interest since they combine the versatility of the surface functionalization with the magnetic properties and the non-toxic biocompatible nature of their core. MNPs are widely adopted for theranostic applications (diagnostic and therapeutic) such as protein and cell sorting and manipulation [8, 9], cell labeling [10, 11], magnetically controlled drug delivery [12, 13], magnetic resonance imaging (MRI) [14, 15], and

* Correspondence: guido.condorelli@unict.it
C. Tudisco and M. T. Cambria contributed equally to this work.
†Equal contributors
[1]Dipartimento di Scienze Chimiche, Università di Catania, 95125 Catania, Italy
[2]INSTM UdR di Catania, 95125 Catania, Italy
Full list of author information is available at the end of the article

© The Author(s). 2018 **Open Access** This article is distributed under the terms of the Creative Commons Attribution 4.0 International License (http://creativecommons.org/licenses/by/4.0/), which permits unrestricted use, distribution, and reproduction in any medium, provided you give appropriate credit to the original author(s) and the source, provide a link to the Creative Commons license, and indicate if changes were made.

hyperthermia [16–19]. To be efficiently used for biomedical applications, MNPs should be capable of crossing cell membranes and, in particular, of passing through the various biological barriers. The modification of the MNPs surface with functional molecules has often been used to improve their cell internalization, but in many cases, the crossing of the BBB remains a problem.

In this context, the use of cell-penetrating peptides (CPPs), a group of relatively short peptides (5–40 amino acids) deriving either from natural sources or from synthetically designed constructs, which can easily cross the membrane bilayer, can be seen as a promising approach. Among the numerous available CPPs, the 20-residue peptide gH625, derived from the glycoprotein H (gH) of the Herpes simplex virus 1, has recently been developed and used to cross the BBB to enhance the uptake of a variety of cargoes [20, 21] into the cytosol.

In the present study, MNPs have been functionalized with two different classes of targeting coatings based both on a coupling layer of 3-aminopropylphosphonic acid (NH_2-PA). The two coatings were obtained by connecting to the NH_2-PA-modified MNPs (NH_2@MNPs) either the gH625 (gH625@MNPs) cell penetrating peptide or PEG and folic acid (PEG,FA@MNPs) molecules. In particular, the introduction of folic acid (FA) into the PEGylated nanoparticles aims at improving both the cellular uptake in tumor cells through FA receptor-mediated internalization [22] and the biocompatibility of the overall nanosystem [23]. The effects of the two surface coatings on MNP intracellular uptake into primary microvascular endothelial cells from human brain (HBMECs) have been evaluated by confocal laser scanning microscopy. To this end, luminescent probes were incorporated into both systems. In particular, gH625 was labeled with the 4-chloro-7-nitrobenz-2-oxa-1,3-diazole (NBD) probe, whilst a carboxy-*X*-rhodamine (rhod) probe was added to the shell of PEG,FA@MNPs.

The study of intracellular uptake of gH625-modified MNPs in endothelial cells and their comparison with FA-modified MNPs, to the best of our knowledge, have never been reported before.

Besides the capability of crossing the BBB, targeting brain tumor cells is another important requirement for brain tumor therapeutic agents. Hence, the cellular internalization of the two differently coated MNPs in one of the most common human malignant glioma, the A-172 glioblastoma, was also evaluated.

Note that though gH625-functionalized iron nanoparticles have recently been prepared by Perillo et al. [24], in the present work, we report a different synthetic strategy based on a highly versatile phosphonic acid platform. In particular, phosphonic acid chemistry allows the formation of strong bonds between MNPs and phosphonic monolayers whose stability is comparable to that of silanized MNP. Moreover, since P-O-P self-condensation is negligible, the use of phosphonic linkers overcomes the oligomer formation drawbacks which are often encountered when using silanes [25].

Methods

Materials

All the reagents used for MNP synthesis and functionalization, $FeCl_2{\cdot}4H_2O$, $FeCl_3{\cdot}6H_2O$, 3-aminopropylphosphonic acid, methoxypolyethylene glycol acetic acid *N*-succinimidyl ester (PEG-NHS) with molecular weight 5000 Da, folic acid, *N*-hydroxysuccinimide (NHS), and carboxy-*X*-rhodamine *N*-succinimidyl ester (Rhod-NHS) were purchased from Sigma-Aldrich and used without further purification. The 9-fluorenylmethoxycarbonyl (Fmoc)-protected amino acids used for the peptide synthesis were purchased by Romil Del Chimica, Chemicals, and were used without further purification. The water was of Milli-Q grade (18.2 MO cm) and was filtered through a 0.22-μm filter.

Synthesis of MNPs

Bare iron oxide MNPs were synthesized by the alkaline co-precipitation of Fe^{3+} and Fe^{2+}, according to the protocol described in the literature [26]. Briefly, $FeCl_2{\cdot}4H_2O$ and $FeCl_3{\cdot}6H_2O$ (molar ratio 1:2) were dissolved in water (50 ml) under an N_2 atmosphere with vigorous stirring. NH_3 25% in H_2O (5 ml) was added to the solution at 80 °C, and the reaction was continued for 30 min. The resulting suspension was cooled to room temperature and washed with ultrapure water. The obtained bare magnetic nanoparticles (bare MNPs) were isolated from the solvent by magnetic decantation.

Synthesis of gH625

The peptide was prepared as previously reported [27] adopting the standard solid phase 9-fluorenylmethoxy carbonyl (Fmoc) method. Briefly, 50 μmol of the peptide was synthesized on a Wang resin (0.75 mmol/g) by consecutive cycles of deprotection and coupling. The resin-bound peptide was then reacted with 4-chloro-7-nitrobenzofurazan (NBD-Cl); the reaction was carried out overnight in the presence of DIPEA. The peptide was cleaved from the resin and deprotected by treatment with a mixture of trifluoroacetic acid (TFA) and scavengers and after precipitated in ice-cold ethylic ether. The peptide was dissolved in water and freeze-dried. The crude peptide characterization was performed by electrospray ionization (ESI) LC-MS adopting a linear gradient of acetonitrile (0.1% TFA) in water (0.1% TFA) from 20 to 80% in 15 min. It was then purified by preparative reversed-phase high-performance liquid chromatography (RP-HPLC).

Synthesis of *N*-Hydroxysuccinimide Ester of Folic Acid (FA-NHS)

FA-NHS was prepared by the following published method [28]. Five hundred milligrams of folic acid (FA) were dissolved in 10 ml of dimethyl sulfoxide (DMSO) with 240 ml of triethylamine. NHS (260 mg) and *N*,*N*-dicyclohexylcarbodiimide (470 mg) were added, and the mixture was reacted overnight at room temperature in the dark. The by-product, dicyclohexylurea, was removed by filtration. The DMSO solution was then concentrated under reduced pressure, and FA-NHS was precipitated in diethyl ether. The product was washed several times with anhydrous ether and dried in air.

Synthesis of Functionalized MNPs

Synthesis of NH_2@MNPs

MNPs (200 mg) were dispersed in H_2O (25 ml) using an ultrasonic bath for 30 min. NH_2-PA (100 mg) was added, and the suspension was agitated for 2 h at room temperature. The particles were separated magnetically and washed four times with H_2O and then with ethanol and dried under air.

Synthesis of gH625@MNPs

NH_2@MNPs (300 mg) and gH625 (1.2 mg) were dispersed in DMSO (20 ml). The solution was mixed overnight at 25 °C. The obtained particles were separated magnetically; washed with DMSO, H_2O, and ethanol; and dried under air.

Synthesis of PEG,FA@MNPs

NH_2@MNPs (300 mg), PEG-NHS (30 mg), FA-NHS (3 mg), and Rhod-NHS (3 mg) were dispersed in DMSO (15 ml), and the solution was mixed overnight at 25 °C. The obtained particles were separated magnetically; washed with DMSO, H_2O, and ethanol; and dried under air.

Sample Characterizations

X-ray powder diffraction (XRD) measurements were performed with a θ–θ 5005 Bruker-AXS diffractometer (Zeiss, Oberkochen, Germany) using Cu Kα radiation operating at 40 kV and 30 mA. X-ray photoelectron spectroscopy (XPS) was performed with a PHI 5600 multi-technique ESCA-Auger spectrometer with a standard Al-Kα X-ray source. Analyses were carried out with a photoelectron angle of 45° (relative to the sample surface) with an acceptance angle of ± 7°. The XPS binding energy (B.E.) scale was calibrated by centering the C 1s peak due to hydrocarbon moieties and adventitious carbon at 285.0 eV. UV/Vis measurements were carried out with a JASCO V-560 UV/Vis spectrophotometer, and the spectra were recorded with a ± 0.2 nm resolution. Dynamic light scattering (DLS) and zeta-potential measurements of MNPs were performed at 25 °C with a Zetasizer Nano-ZS (Malvern Instruments, Malvern, UK) equipped with He–Ne laser (633 nm) and a backscatter detector (173°). Transmission FT-IR measurements were recorded with a JASCO FTIR 430 spectrometer, using the KBr pellet technique, with 100 scans collected per spectrum (scan range 560–4000 cm^{-1}, resolution 4 cm^{-1}).

Cell Culture

Human brain microvascular endothelial cells (HBMEC) and human glioblastoma cell line A-172 were grown to confluence in rat-tail collagen type I-coated tissue culture flasks, according to the reported method [29]. Briefly, HBMEC were grown in the endothelial cell medium supplemented with 5% fetal bovine serum (FBS) and 1% endothelial cell growth supplement. A-172 cell line was grown in DMEM containing 2 mM glutamine and 10% FBS as previously described [30]. In both cases, 100 U/ml penicillin and 100 μg/ml streptomycin were also added to the cultures.

Cell Viability Assay

Cell viability was determined with the [3-(4,5-dimethyl-2-thiazolyl)-2,5-diphenyl-2*H*-tetrazolium bromide] (MTT) test [31]. In all experimental conditions, the FBS concentration was reduced to 1% (starving medium). Cells were seeded in 96-well plates at 7000 cells/well to obtain optimal cell density throughout the experiment. In all assays, cells were first incubated at 37 °C with MTT for 3 h; then, isopropanol with 0.04 M HCl was added, and the absorbance was measured at 1 h in a plate reader (Synergy 2-Bio-Tek) with a test wavelength of 570 nm [32].

Confocal Microscopy

Confocal microscopy was performed on both HBMEC and A-172 glioblastoma cells grown on microscope cover glasses placed in a 24-well plate. After incubations with or without MNPs, cells were fixed by adding 4% paraformaldehyde in PBS and processed for immunocytochemistry as early described [33]. Confocal microscopy analyses were carried out with an Olympus FV1000 confocal laser scanning microscope (LSM) equipped with the following excitation sources: diode laser (405 nm), multiline Ar laser (457, 488, and 515 nm), HeNe(G) laser (543 nm), and HeNe(R) laser (633 nm). An oil immersion objective (60xO PLAPO) was used, and the emitted light was detected in sequential mode through a spectral filtering system. The detector gain was fixed at a constant value, and images were taken for all of the samples at random locations throughout the area of the well. The following acquisition parameters were used: λex/em = 405/425 – 475 nm (blue channel, nuclear staining by DAPI); λex/em = 488/500 – 530 nm (green channel, gH625@MNPs labelling by NBD); and λex/em = 633/650 – 700 nm (red channel, PEG,FA@MNPs labelling by rhod). Quantitative analysis of fluorescence was performed by using the ImageJ software (1.50i version, NIH).

Results and Discussion

Synthesis and Characterization of MNPs

The overall strategy implemented to prepare gH625@MNPs and PEG,FA@MNPs from Fe_3O_4 nanoparticles, obtained by co-precipitation, involves two steps as illustrated in Fig. 1. The first step, which is the same for both classes of nanoparticles, is based on the MNP functionalization with a phosphonic acid bearing an amino group (NH_2-PA). In the second step, the NH_2-PA-prefunctionalized MNPs (NH_2@MNPs) are further conjugated with specific functional molecules via NHS coupling reactions. In particular, the *N*-hydroxysuccinimide-activated form of gH625 labeled with NBD was used for the preparation of gH625@MNPs, and *N*-hydroxysuccinimide activated forms of PEG, FA, and Rhod were used to obtain PEG,FA@MNPs. Note that both gH625@MNPs and PEG,FA@MNPs have been labeled with luminescent probes (i.e., NBD and Rhod, respectively) in order to carry out confocal laser scanning microscopy studies.

The X-ray diffractometric (XRD) characterization of bare MNPs obtained after the co-precipitation step is similar to that reported in our previous papers [34, 35]. Briefly, a typical pattern (Fig. 2a) shows four diffraction peaks ($2\theta = 30.16°$, $35.48°$, $43.10°$, and $57.04°$) which is consistent with the presence of magnetite, maghemite, or any intermediate composition between the two phases. The lattice constant, a, that was found to be 8.389(4) Å in good agreement with the lattice parameter of bulk magnetite (8.396 Å), as well as the average crystal size of 11.2, determined applying the Debye–Scherrer's equation, are comparable with the values previously reported [34, 35].

Note that since the crystal structure of Fe_3O_4 magnetite is very similar to that of γ-Fe_2O_3 maghemite, it is very difficult to distinguish the two phases by XRD. For this reason, X-ray photoelectron spectroscopy (XPS) was used to further analyze the MNPs. Figure 2b shows Fe $2p_{3/2}$ high-resolution XPS spectra of bare MNPs. The centroid of the band, observed at 710.9 eV, corresponds to the Fe $2p_{3/2}$ peak. This value is lower than that reported for Fe^{3+} either in octahedral holes of α-Fe_2O_3 (711.6 eV) [36, 37] or in mixed tetrahedral and octahedral holes of γ-Fe_2O_3 (711.4 eV), and it is consistent with the mixed oxidation state of Fe in Fe_3O_4 [37, 38].

Finally, a detailed magnetic characterization of similar MNPs is reported in our previous papers [34, 35].

The functionalization process was evaluated by FT-IR and XPS. After functionalization with phosphonic monolayers, the Fe $2p_{3/2}$ band (Fig. 2c) does not show relevant modifications, thus confirming that the Fe_3O_4 phase is retained. However, a slight shift (0.4 eV) of the Fe $2p_{3/2}$ centroid towards lower binding energy (B.E) was observed, which was associated to the anchoring of the phosphonic monolayer. Similar shifts were, in fact, observed in phosphate adsorption of various ferric oxides [39] and can be ascribed to some charge transfer from adsorbate to Fe atoms. The Fe $2p_{3/2}$ position of 710.5 eV was maintained after all the functionalization steps for the anchoring of PEG and FA.

Figure 3 reports the comparison of P2p, N1s, and C 1s spectral regions of NH_2@MNPs, PEG,FA@MNPs, and gH625@MNPs, respectively. The P2p peak position (133.2 eV) of NH_2@MNPs is typically associated with the presence of the phosphonic acid anchored on the

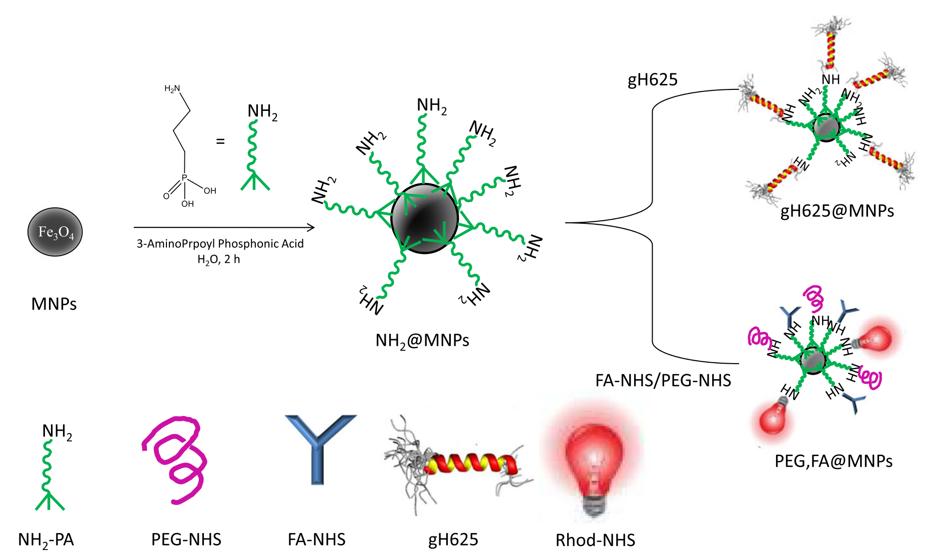

Fig. 1 Reaction scheme. Reaction steps for the preparation of functionalized MNPs

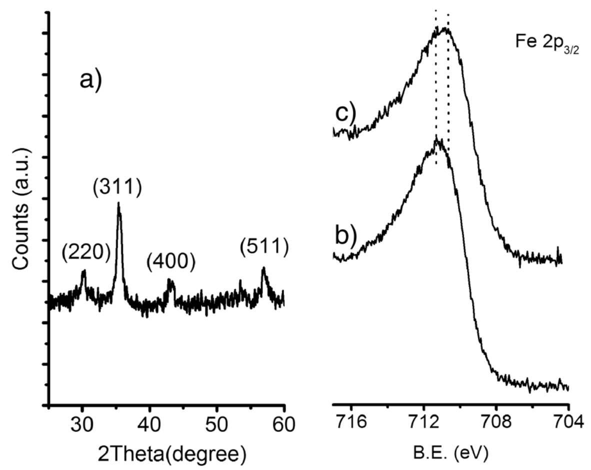

Fig. 2 Typical XRD and XPS spectra of MNPs. XRD pattern of a) bare MNPs and high-resolution Fe $2p_{3/2}$ XPS spectral regions of b) bare MNPs and c) NH_2@MNPs

surface in a bidentate way [40–43]. The P2p band position in the spectra of gH625@MNPs and PEG,FA@MNPs is the same of that observed in NH_2@MNPs spectrum, thus revealing that the phosphonic molecules are not removed during the coupling reactions for the peptide and folic acid immobilization.

The shape and the peak position of N1s spectra of NH_2@MNPs are consistent with the presence of the anchored NH_2-PA. The band consists of two distinct components: the first one at 399.9 eV is associated with the –NH groups of the anchored aminopropylphosphate, and the second component centered at 401.5 eV is due to the amino groups interacting with the surface of Fe_3O_4 through protonation or formation of –H bonds.

After the anchoring of either gH625 peptide or FA, PEG, and Rhod, the N1s component at 399.8 eV

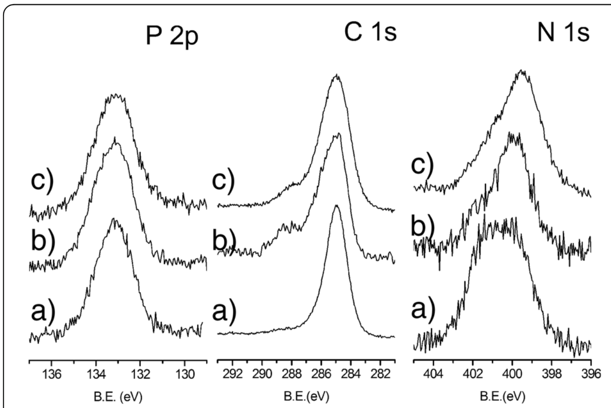

Fig. 3 XPS characterization of functionalized MNPs. High-resolution P 2p, C 1s, and N 1s XPS spectral regions of a) NH_2@MNPs, b) PEG,FA@MNPs, and c) gH625@MNPs

increases compared with the component at 401.8 eV related to protonated amino moieties of NH_2@MNPs. This increment is due to the overlapped signals of the N atoms involved in the amidic bond (400.2 eV) between the anchored aminopropylphosphate and the conjugated molecules (e.g., gh625, FA, PEG, and Rhod) as well as of the N atoms of gh625 and FA (at 399.1 and 400.6 eV).

The C 1s band of NH_2@MNPs spectrum consists of a single peak at 285.0 eV assigned to aliphatic carbons, as previously reported [40].

In the C1s spectra of gH625@MNPs and PEG,FA@MNPs, the presence of a C 1s component at 288.3 eV is due to the carboxylic and amidic groups of gh625, FA, and Rhod molecules.

FT-IR spectra of NH_2@MNPs, gH625@MNPs, and PEG,FA@MNPs are reported in Fig. 4. In all samples, spectra do not show the bands at 1250 cm^{-1} due to P=O and the sharp peaks in the 900–1050 cm^{-1} ranges due to P–O–H stretching [44–46], but a broad and strong band at 1040 cm^{-1}, which is associated to the vibrations of the PO_3^{2-} group bonded to the iron surface. This band indicates, according to XPS results, that the phosphonic acids are deprotonated and are anchored to the surface through P–O–Fe bondings as previously reported [34, 40, 41]. The IR spectral region between 1500 and 1700 cm^{-1} shows the bands belonged to the amino and amide groups of gH625 and FA. In particular, spectrum of NH_2@MNPs shows a sharp peak around 1650 cm^{-1} associated to the NH_2 bending [47]. After PEG, Rhod, and FA anchoring, 1700–1500 cm^{-1} region of PEG,FA@MNPs shows broader bands due to the convolution of the vibrations of unreacted NH_2, amide groups, and benzene rings of FA and Rhod (1630–1600 cm^{-1}) [35]. Analogously, after peptide anchoring, the broad bands at about 1650–1600 cm^{-1} can be due to the contribution of several vibrations due to unreacted NH_2 and aminic moieties of the peptide side chains and to the C=O stretch of the peptide amidic bonds [48]. In addition, a component at about 1540 cm^{-1} due to the combined δ(N–H)/ν(C–N) vibrations of the peptide [48] is also present.

The FA anchoring on MNPs has also been proved by the UV/Vis spectra of a PEG,FA@MNPs colloidal solution. Figure 5 compares the spectra of NH_2@MNPs and PEG,FA@MNPs colloidal dispersions. The spectrum of a FA solution (5 μM) has been added as a reference. An evident band at 274 nm typical of the FA is clearly visible in both the reference and the PEG,FA@MNPs colloidal solution, thus confirming the presence of FA in the MNPs. Note that the slight shift is from the FA-NHS absorption at 280 nm to the value of 274 nm after anchoring is likely due to the change of the environment from free FA-NHS and nanoparticle-anchored FA. The presence of variable shifts of the absorption band at

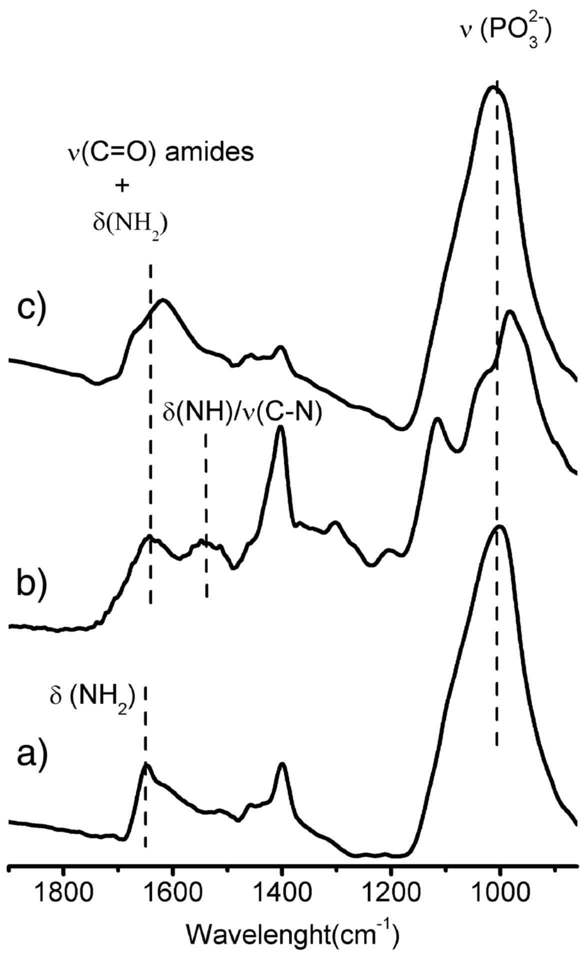

Fig. 4 FT-IR characterization of functionalized MNPs. FT-IR spectral region in the 850–1900 cm^{-1} range of a) NH_2@MNPs, b) gH625@MNPs, and c) PEG,FA@MNPs

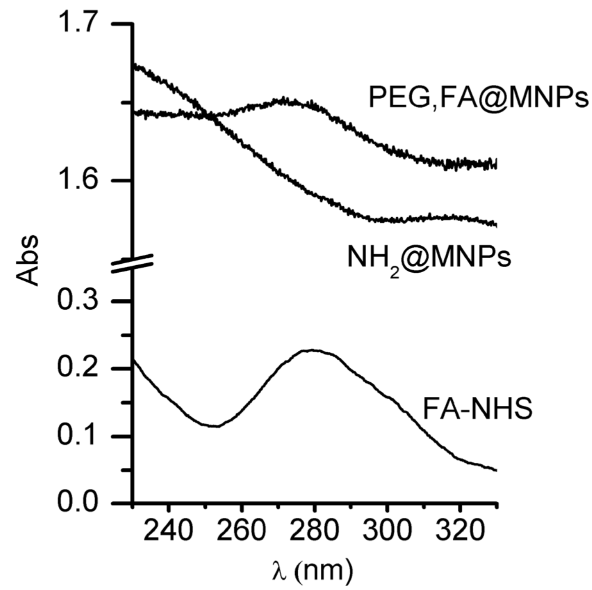

Fig. 5 UV/Vis characterization of functionalized MNPs. UV/Vis spectra of a 5 μM FA-NHS solution and of NH_2@MNPs, and PEG,FA@MNPs colloidal dispersions. Note that the high background observed in the spectra of NH_2@MNPs and PEG,FA@MNPs is due to the scattering of the nanoparticle colloidal dispersion

280 nm after FA surface anchoring or conjugation with other molecules has been already observed in literature [49–51].

The mean hydrodynamic diameter, the polydispersity index (PDI), and the zeta potential of functionalized MNPs were determined by DLS in PBS buffer at pH 7.4 on MNP dispersions as prepared and after 72 h of aging (Table 1). The hydrodynamic diameters of NH_2-PA@MNPs, gH625@MNPs, and PEG,FA@MNPs were 73.0 ± 3.0 nm, 104.0 ± 4.0 nm, and 51 ± 2 nm, respectively, and PDI values indicate a narrow enough distribution of the particle size. As expected, the conjugation with gH625 increased the size of nanoparticles, while the decrement in the size of PEG,FA@MNPs is due to a better dispersion than the NH_2@MNPs, related to the presence of the PEG chains.

In any case, note that highly negative zeta potential (< − 30 mV) were observed for all systems. Such negative zeta potential values ensure long-term stability and avoid extensive particle aggregation [52, 53]. Indeed, the negative surface charge was only slightly dependent on the coating but mainly resulted from the combination of the negatively charged core of Fe_3O_4 nanoparticles [54] and the effect of phosphonic acid groups as observed for similar systems [52, 34]. Therefore, compared to other synthetic strategies used to functionalize MNPs, the use of phosphonic acid monolayers as linkers not only allows the formation of stable bonding between the surface and the functional groups, but also induces highly negative zeta potential. After 72 h of aging, the size and zeta potential of NH_2-PA@MNPs, gH625@MNPs, and PEG,FA@MNPs remain approximatively the same, suggesting that all decorated surfaces are stable over time.

Table 1 Mean hydrodynamic diameter, polydispersity index (PDI), and zeta potential of functionalized MNPs determined by DLS in PBS as prepared and after 72 h of aging

	NH_2@MNPs		gH625@MNPs		PEG,FA@MNPs	
	0 h	72 h	0 h	72 h	0 h	72 h
Size (nm)	73 ± 3	71 ± 4	104 ± 4	109 ± 4	51 ± 2	52 ± 6
PDI	0.23	0.22	0.18	0.20	0.34	0.37
ζ (mV)	− 44 ± 1	− 46 ± 1	− 45 ± 1	− 45 ± 1	− 42 ± 1	− 42 ± 1

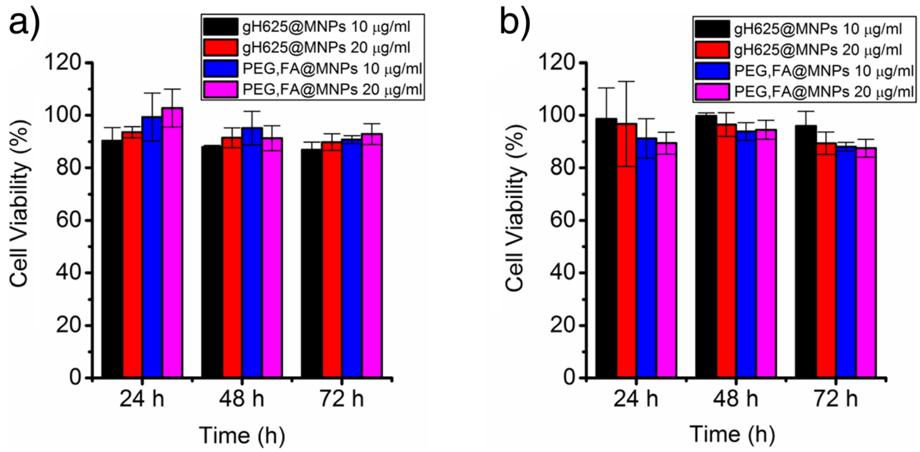

Fig. 6 Cell viability. Cell viability of **a** HBMEC and **b** A-172 cells incubated for 24, 48, and 72 h with gH625@MNPs 10 μg/ml (black bar), gH625@MNPs 20 μg/ml (red bar), PEG,FA@MNPs 10 μg/ml (blue bar), and PEG,FA@MNPs 20 μg/ml (magenta bar)

Cell Viability

The viability of HBMEC and A-172 cells incubated with gH625@MNPs and FA,PEG@MNPs was evaluated using MTT assay at different incubation times and in the presence of different concentrations of nanoparticles (10 and 20 μg/ml). As shown in Fig. 6, no concentration and/or time-dependent (24–48–72 h) cytotoxic effect of the decorated systems on HBMEC and A-172 cells was observed.

Intracellular Uptake

In order to determine whether the cell-penetrating capability of gH625 peptide is retained after its immobilization at the nanoparticle surface, and to compare the gH625 and FA capability of crossing the BBB, the internalization into human brain endothelial cells of NBD-labeled gH625@MNPs and Rhod-labeled PEG,-FA@MNPs has been investigated with confocal laser scanning microscopy.

After 24 h of incubation, the uptake of PEG-FA@MNPs is not evident, while gH625@MNPs internalization is clearly visible (Fig. 7). The conjugation with gH625 leads to a more rapid uptake and a nearly twofold higher intensity of the intracellular fluorescence (Fig. 8).

For longer times of incubation (72 h), differences between the internalization of the two systems are reduced. This behavior is not unexpected since for long incubation times, unspecific internalization processes of FA,PEG@MNPs can occur and our results further confirm what we previously reported for the uptake of functionalized and unfunctionalized polystyrene nanoparticles [55].

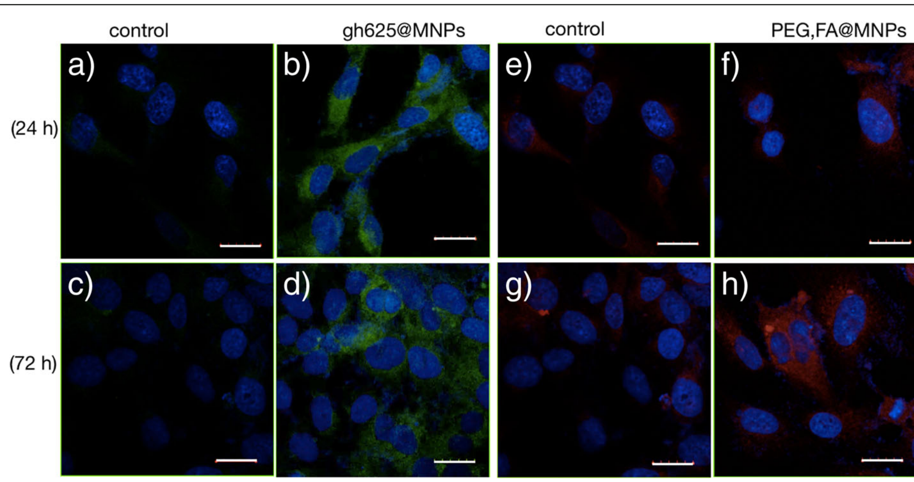

Fig. 7 LSM fluorescence micrographs of HBMEC. LSM fluorescence micrographs of HBMEC incubated for 24 h (**b**, **f**) and 72 h (**d**, **h**) with NBD-labelled gH625@MNPs 15 μg/ml (**b**, **d**) and their controls (**a**, **c**) or rhod-labeled PEG,FA@MNPs 15 μg/ml (**f**, **h**) and their controls (**e**, **g**). Scale bar = 20 μm

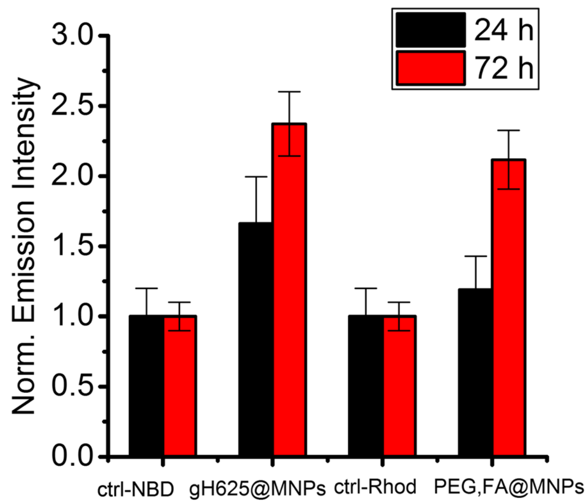

Fig. 8 Normalized intensities of intracellular fluorescence. Quantitative analysis of intracellular fluorescence after HBMEC incubation at 24 and 72 h with NBD-labeled gH625@MNPs and Rhod-labeled FA,PEG@MNPs

To further explore the possibility of using gH625@MNPs as a therapeutic agent for brain tumors, the cellular uptakes of gH625@MNPs and FA,PEG@MNPs were investigated using the A-172 glioblastoma cell line. Glioblastoma is one of the most common primary brain tumor and also one of the most lethal cancers.

The cellular uptakes of gH625@MNPs and FA, PEG@MNPs after 24 h of incubation are comparable, as shown in Fig. 9.

This behavior suggests that the gH625 is capable of targeting brain tumor with the same efficiency of the more often adopted FA targeting unit.

Conclusions

Fe_3O_4 nanoparticles have been functionalized with the gH625 viral cell penetrating peptide adopting a versatile route based on MNP prefunctionalization with a monolayer consisting of a bifunctional phosphonic linker, 3-aminopropylphosphonic acid. The cell internalization capabilities of this system have been evaluated by comparing them with those of a reference system based on MNPs functionalized with PEG, rhodamine, and folic acid, obtained adopting the same NH_2-PA-based platform. The uptake of the two differently decorated MNPs was assessed in primary microvascular endothelial cells from human brain, which are the main components of the BBB and simulate an in vitro model of the BBB. These surface modifications influence the internalization of MNPs in HBMEC and, therefore, their capability to cross the BBB. In fact, conjugation with the gH625 peptide upgraded the delivery of nanoparticles across the in vitro BBB, leading to significant higher cell uptake in HBMEC after 24 h compared with that of FA bearing MNPs (FA,PEG@MNPs). Note that also other strategies have been used to enhance nanoparticle uptake across the BBB. A common approach is to attach targeting ligands in order to activate receptor-mediated endocytosis. As examples, transferrin-coupling nanoparticles can penetrate into the BBB through a transferrin receptor-mediated process [56]. Analogously, the linkage of the apolipoprotein E to the nanoparticles enhances the BBB penetration [57]. Besides, nanoparticles having a surface charges modified with polyethylenimine (PEI) has been reported to cross the BBB by absorptive-mediated transcytosis [58]. Finally, the ability of MNPs to pass through human brain microvascular endothelial cells, used as an in vitro BBB model, can be also facilitated by an external magnet [59]. In our work, we studied a different approach which use a cell penetrating peptide, the gh625, to improve internalization capabilities of Fe_3O_4 nanoparticles. These results are in accordance with those previously obtained by D. Guarnieri et al. using different kinds of MNPs [55, 60] confirming that the gH625-decorated magnetic nanoparticle has a relevant role in crossing the BBB and could be used as a safe and effective drug delivery system.

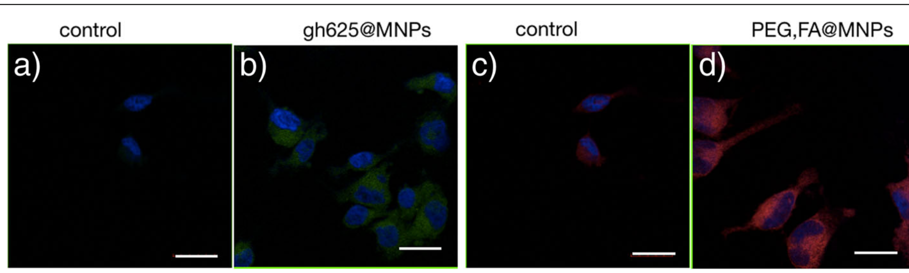

Fig. 9 LSM fluorescence micrographs of glioblastoma cells. LSM fluorescence micrographs of glioblastoma cells. Merged blue-green images: control cells (**a**) and cells incubated with 15 μg/ml of NBD-labeled gH625@MNPs (**b**). Merged blue-red images: control cells (**c**) and cells incubated with 15 μg/ml rhod-labeled PEG,FA@MNPs (**d**). Scale bar = 20 μm

Abbreviations
A-172: Human glioblastoma cell line; B.E.: Binding energy; BBB: Blood-brain barrier; CNS: Central nervous system; CPPs: Cell-penetrating peptides; DIPEA: *N,N*-Diisopropylethylamine; DLS: Dynamic light scattering; DMEM: Dulbecco's modified Eagle's medium; DAPI: 4′,6-Diamidino-2-phenylindole; DMSO: Dimethyl sulfoxide; FA: Folic acid; FA-NHS: Activated form of FA with NHS; FBS: Fetal bovine serum; Fmoc: 9-Fluorenylmethoxycarbonyl; FT-IR: Fourier transform infrared spectroscopy; gh625: 20-Residue peptide derived from the glycoprotein H (gH) of the Herpes simplex virus 1; gH625@MNPs: NH_2@MNPs functionalized with gh625; HBMECs: Microvascular endothelial cells from human brain; MNPs: Magnetic iron nanoparticles; MTT: 3-(4,5-Dimethyl-2-thiazolyl)-2,5-diphenyl-2*H*-tetrazolium bromide; NBD: 4-Chloro-7-nitrobenz-2-oxa-1,3-diazole; NH_2@MNPs: MNPs modified with NH_2-PA; NH_2-PA: 3-Aminopropylphosphonic acid; NHS: *N*-Hydroxysuccinimide; PBS: Phosphate-buffered saline; PDI: Polydispersity index; PEG: Polyethylene glycol; PEG,FA@MNPs: NH_2@MNPs functionalized with FA, Rhod and PEG; PEG-NHS: Methoxypolyethylene glycol acetic acid *N*-succinimidyl ester; PEI: Polyethylenimine; Rhod: Carboxy-*X*-rhodamine; Rhod-NHS: Carboxy-*X*-rhodamine *N*-succinimidyl ester; TFA: Trifluoroacetic acid; XPS: X-ray photoelectron spectroscopy; XRD: X-ray powder diffraction

Funding
The authors thank the University of Catania for the financial support within the FIR A19DBF project.

Availability of Data and Materials
Not applicable

Authors' Contributions
CT, MTC, and GGC coordinated this study; CT, MTC, FS, CDA, GL, AF, SG, VO, CS, and GGC wrote the paper. AF and SG carried out the synthesis and characterization of the gH625 peptide; CT and AEG carried out the nanoparticle synthesis and functionalization; CT, AEG, and GGC performed the chemical and structural characterization of functionalized MNPs; CDA, GL, and NC performed experiments with HBMEC and A-172 cell lines. MTC and FS performed cell viability studies; CS performed the confocal microscopy study; VO performed the DLS and zeta potential measurements. All authors commented on the manuscript. All authors read and approved the final manuscript.

Competing Interests
The authors declare that they have no competing interests.

Publisher's Note
Springer Nature remains neutral with regard to jurisdictional claims in published maps and institutional affiliations.

Author details
[1]Dipartimento di Scienze Chimiche, Università di Catania, 95125 Catania, Italy. [2]INSTM UdR di Catania, 95125 Catania, Italy. [3]Dipartimento di Scienze Biomediche e Biotecnologiche, Università di Catania, 95100 Catania, Italy. [4]Dipartimento di Farmacia, Università di Napoli "Federico II", 80134 Napoli, Italy.

Received: 7 September 2017 Accepted: 26 January 2018
Published online: 07 February 2018

References
1. Nico B, Ribatti D (2012) Morphofunctional aspects of the blood–brain barrier. Curr Drug Metab 13:50–60
2. Bernacki J, Dobrowolska A, Nierwińska K, Malecki A (2008) Physiology and pharmacological role of the blood–brain barrier. Pharmacol Rep 60:600–622
3. Braun LD, Cornford EM, Oldendorf WH (1980) Newborn rabbit blood-brain barrier is selectively permeable and differs substantially from the adult. J Neurochem 34:147–152
4. Stanimirovic DB, Friedman A (2012) Pathophysiology of the neurovascular unit: disease cause or consequence? J Cereb Blood Flow Metab 32:1207–1221
5. Hawkins BT, Davis TP (2005) The blood-brain barrier/neurovascular unit in health and disease. Pharmacol Rev 57:173–185
6. Pardridge WM (2005) The blood-brain barrier: bottleneck in brain drug development. NeuroRx 2:3–14
7. Di Pietro P, Caporarello N, Anfuso CD, Lupo G, Magrì A, La Mendola D, Satriano C (2017) Immobilization of neurotrophin peptides on gold nanoparticles by direct and lipid-mediated interaction: a new multipotential therapeutic nanoplatform for CNS disorders. ACS Omega 2:4071–4079
8. Pan Y, Du X, Zhao F, Xu B (2012) Magnetic nanoparticles for the manipulation of proteins and cells. Chem Soc Rev 41:2912–2942
9. Huang Z, Pei N, Wang Y, Xie X, Sun A, Shen L, Zhang S, Liu X, Zou Y, Qian J, Ge J (2010) Deep magnetic capture of magnetically loaded cells for spatially targeted therapeutics. Biomaterials 31:2130–2140
10. Wilhelm C, Gazeau F (2008) Universal cell labelling with anionic magnetic nanoparticles. Biomaterials 29:3161–3174
11. Neoh KG, Kang ET (2012) Surface modification of magnetic nanoparticles for stem cell labeling. Soft Matter 8:2057–2069
12. N'Guyen TTT, Duong HTT, Basuki J, Montembault V, Pascual S, Guibert C, Fresnais J, Boyer C, Whittaker MR, Davis TP, Fontaine L (2013) Functional iron oxide magnetic nanoparticles with hyperthermia-induced drug release ability by using a combination of orthogonal click reactions. Angew Chem Int Ed Engl 52:14152–14156
13. Mody VV, Cox A, Shah S, Singh A, Bevins W, Parihar H (2014) Magnetic nanoparticle drug delivery systems for targeting tumor. Appl Nanosci 4:385–392
14. Arosio P, Thévenot J, Orlando T, Orsini F, Corti M, Mariani M, Bordonali L, Innocenti C, Sangregorio C, Oliveira H, Lecommandoux S, Lascialfari A, Sandre O (2013) Hybrid iron oxide-copolymer micelles and vesicles as contrast agents for MRI: impact of the nanostructure on the relaxometric properties. J Mater Chem B 1:5317–5328
15. Tassa C, Shaw SY, Weissleder R (2011) Dextran-coated iron oxide nanoparticles: a versatile platform for targeted molecular imaging, molecular diagnostics, and therapy. Acc Chem Res 44:842–852
16. Troyer DL, Bossman SH (2012) Utilization of magnetic nanoparticles for cancer therapy. In: Srirajaskanthan RP, Victor R, (editors). Nanomedicine and cancer. Enfield: Science Publishers, Inc., p 84–104
17. Creixell M, Bohòrquez AC, Torres-Lugo M, Rinaldi C (2011) EGFR-targeted magnetic nanoparticle heaters kill cancer cells without a perceptible temperature rise. ACS Nano 5:7124–7129
18. Yoo D, Jeong H, Noh SH, Lee JH, Cheon J (2013) Magnetically triggered dual functional nanoparticles for resistance-free apoptotic hyperthermia. Angew Chem Int 52:13047–13051
19. Fantechi E, Innocenti C, Zanardelli M, Fittipaldi M, Falvo E, Carbo M, Shullani V, Di Cesare ML, Ghelardini C, Ferretti AM, Ponti A, Sangregorio C, Ceci P (2014) A smart platform for hyperthermia application in cancer treatment: cobalt-doped ferrite nanoparticles mineralized in human ferritin cages. ACS Nano 8:4705–4719
20. Galdiero S, Falanga A, Morelli G, Galdiero M (2015) gH625: a milestone in understanding the many roles of membranotropic peptides. Biochim Biophys Acta 1848:16–25
21. Galdiero S, Falanga A, Vitiello M, Grieco P, Caraglia M, Morelli G, Galdiero M (2014) Exploitation of viral properties for intracellular delivery. J Pept Sci 20:468–478
22. Tang Z, Li D, Sun H, Guo X, Chen Y, Zhou S (2014) Quantitative control of active targeting of nanocarriers to tumor cells through optimization of folate ligand density. Biomaterials 35:8015–8027
23. Sun J, Zhou S, Hou P, Yang Y, Weng J, Li X, Li M (2007) Synthesis and characterization of biocompatible Fe3O4 nanoparticles. J Biomed Mater Res A 80:333–341
24. Perillo E, Hervé-Aubert K, Allard-Vannier E, Falanga A, Galdiero S, Chourpa I (2017) Synthesis and *in vitro* evaluation of fluorescent and magnetic nanoparticles functionalized with a cell penetrating peptide for cancer theranosis. J Colloid Interface Sci 499:209–217
25. Turcheniuk K, Tarasevich AV, Kukhar VP, Boukherroub R, Szunerits S (2013) Recent advances in surface chemistry strategies for the fabrication of functional iron oxide based magnetic particles. Nano 5:10729–10752
26. Peng ZG, Hidajat K, Uddin MSJ (2004) Adsorption of bovine serum albumin on nanosized magnetic particles. J Colloid Interface Sci 271:277–283
27. Galdiero S, Falanga A, Vitiello M, Raiola L, Russo L, Pedone C, Isernia C, Galdiero M (2010) The presence of a single N-terminal histidine residue enhances the fusogenic properties of a membranotropic peptide derived from herpes simplex virus type 1 glycoprotein H. J Biol Chem 285:17123–17136

28. Lee RJ, Low PS (1994) Delivery of liposomes into cultured KB cells via folate receptor-mediated endocytosis. J Biol Chem 5:3198–3204
29. Caporarello N, Olivieri M, Cristaldi M, Scalia M, Toscano MA, Genovese C, Addamo A, Salmeri M, Lupo G, Anfuso CD (2017) Blood–brain barrier in a Haemophilus influenzae type a in vitro infection: role of adenosine receptors A2A and A2B. Mol Neurobiol. doi: https://doi.org/10.1007/s12035-017-0769-y
30. Esteve PO, Tremblay P, Houde M, St-Pierre Y, Mandeville R (1998) In vitro expression of MMP-2 and MMP-9 in glioma cells following exposure to inflammatory mediators. Biochim Biophys Acta 1403:85–96
31. Mosmann T (1983) Rapid colorimetric assay for cellular growth and survival: application to proliferation and cytotoxicity assays. J Immunol Methods 65:55–63
32. Lupo G, Assero G, Anfuso CD, Nicotra A, Palumbo M, Cannavo G, Renis M, Ragusa N, Alberghina M (2002) Cytosolic phospholipase A2 mediates arachidonoyl phospholipid hydrolysis in immortalized rat brain endothelial cells stimulated by oxidized LDL. Biochim Biophys Acta 1585:19–29
33. Anfuso CD, Lupo G, Romeo L, Giurdanella G, Motta C, Pascale A, Tirolo C, Marchetti B, Alberghina M (2007) Endothelial cell-pericyte cocultures induce PLA2 protein expression through activation of PKC and the MAPK/ERK cascade. J Lipid Res 48:782–793
34. Tudisco C, Bertani F, Cambria MT, Sinatra F, Fantechi E, Innocenti C, Sangregorio C, Dalcanale E, Condorelli GG (2013) Functionalization of PEGylated Fe_3O_4 magnetic nanoparticles with tetraphosphonate cavitand for biomedical application. Nano 5:11438–11446
35. Tudisco C, Cambria MT, Sinatra F, Bertani F, Alba A, Giuffrida AE, Saccone S, Fantechi E, Innocenti C, Sangregorio C, Dalcanale E, Condorelli GG (2015) Multifunctional magnetic nanoparticles for enhanced intracellular drug transport. J Mater Chem B 3:4134–4145
36. Mills P, Sullivan JL (1983) A study of the core level electrons in iron and its three oxides by means of X-ray photoelectron spectroscopy. J Phys D Appl Phys 16:723–732
37. Fujii T, de Groot F, Sawatzky MF, Voogt GA, Hibma FC, Okada TK (1999) *In situ* XPS analysis of various iron oxide films grown by NO2-assisted molecular-beam epitaxy. Phys Rev B 59:3195–3202
38. Hayashi K, Ono K, Suzuki H, Sawada M, Moriya M, Sakamoto W, Yogo T (2010) High-frequency, magnetic-field-responsive drug release from magnetic nanoparticle/organic hybrid based on hyperthermic effect. ACS Appl Mater Interfaces 2:1903–1911
39. Dinghua Y, Wu C, Kong Y, Xue N, Guo X, Ding W (2007) Structural and catalytic investigation of mesoporous iron phosphate. J Phys Chem C 111:14394–14399
40. Tudisco C, Oliveri V, Cantarella M, Vecchio G, Condorelli GG (2012) Cyclodextrin anchoring on magnetic Fe_3O_4 nanoparticles modified with phosphonic linkers. Eur J Inorg Chem 32:5323–5331
41. Smecca E, Motta A, Fragalà ME, Aleeva Y, Condorelli GG (2013) Spectroscopic and theoretical study of the grafting modes of phosphonic acids on ZnO nanorods. J Phys Chem C 117:5364–5372
42. Textor M, Ruiz L, Hofer R, Rossi A, Feldman K, Hahner G, Spencer ND (2000) Structural chemistry of self-assembled monolayers of octadecylphosphoric acid on tantalum oxide surfaces. Langmuir 16:3257–3271
43. Chen Y, Liu W, Ye C, Yu L, Qi S (2001) Preparation and characterization of self-assembled alkanephosphate monolayers on glass substrate coated with nano-TiO2 thin film. Mater Res Bull 36:2605–2612
44. Zhang B, Kong T, Xu W, Su R, Gao Y, Cheng G (2010) Surface functionalization of zinc oxide by carboxyalkylphosphonic acid self-assembled monolayers. Langmuir 26:4514–4522
45. Dembereldorj U, Ganbold EO, Seo JH, Lee SY, Yang S, Joo SW (2012) Conformational changes of proteins adsorbed onto ZnO nanoparticle surfaces investigated by concentration-dependent infrared spectroscopy. Vib Spectrosc 59:23–28
46. Luschtinetz R, Seifert G, Jaehne E, Adler HJP (2007) Infrared spectra of alkylphosphonic acid bound to aluminium surfaces. Macromol Symp 254:248–253
47. Manju S, Sharma CP, Sreenivasan K (2011) Targeted coadministration of sparingly soluble paclitaxel and curcumin into cancer cells by surface engineered magnetic nanoparticles. J Mater Chem 21:15708–15717
48. Barth A (2007) Infrared spectroscopy of proteins. Biochim Biophys Acta 1767:1073–1101
49. Lebret V, Raehm L, Durand JO, Smaïhi M, Werts MHV, Blanchard-Desce M, Me'thy-Gonnod D, Dubernet C (2008) Surface functionalization of two-photon dye-doped mesoporous silica nanoparticles with folic acid: cytotoxicity studies with HeLa and MCF-7 cancer cells. J Sol-Gel Sci Technol 48:32–39
50. Du P, Yang H, Zeng J, Liu P (2013) Folic acid-conjugated temperature and pH dual responsive yolk/shell microspheres as a drug delivery system. J Mater Chem B 1:5298–5308
51. Ghanbari M, Asadi A, Rostamzadeh S (2016) Study of the cytotoxicity effect of doxorubicin-loaded/folic acid-targeted super paramagnetic iron oxide nanoparticles on AGS cancer cell line. J Nanomed Nanotechnol 7:368
52. Benyettou F, Lalatonne Y, Chebbi I, Di Benedetto M, Serfaty JM, Lecouvey M, Motte L (2011) A multimodal magnetic resonance imaging nanoplatform for cancer theranostics. Phys Chem Chem Phys 13:10020–10027
53. Feng S, Huang GJ (2001) Effects of emulsifiers on the controlled release of paclitaxel (Taxol®) from nanospheres of biodegradable polymers. Control Release 71:53–69
54. Mohapatra S, Pramanik P (2009) Synthesis and stability of functionalized iron oxide nanoparticles using organophosphorus coupling agents. Colloids Surf A Physicochem Eng Asp 339:35–42
55. Guarnieri D, Falanga A, Muscetti O, Tarallo R, Fusco S, Galdiero M, Galdiero S, Netti PA (2013) Shuttle-mediated nanoparticle delivery to the blood-brain barrier. Small 9:853–862
56. Clark AJ, Davis ME (2015) Increased brain uptake of targeted nanoparticles by adding an acid-cleavable linkage between transferrin and the nanoparticle core. Proc Natl Acad Sci U S A 112:12486–12491
57. Neves AR, Queiroz JF, Lima SAC, Reis S (2017) Apo E-functionalization of solid lipid nanoparticles enhances brain drug delivery: uptake mechanism and transport pathways. Bioconjug Chem 28(4):995–1004
58. Georgieva JV, Kalicharan D, Couraud PO, Romero IA, Weksler B, Hoekstra D, Zuhorn IS (2011) Surface characteristics of nanoparticles determine their intracellular fate in and processing by human blood-brain barrier endothelial cells in vitro. Mol Ther 19:318–325
59. Thomsen LB, Linemann T, Pondman KM, Lichota J, Kim KS, Pieters RJ, Visser GM, Moos T (2013) Uptake and transport of superparamagnetic iron oxide nanoparticles through human brain capillary endothelial cells. ACS Chem Neurosci 4:1352–1360
60. Guarnieri D, Muscetti O, Falanga A, Fusco S, Belli V, Perillo E, Battista E, Panzetta V, Galdiero S, Netti PA (2015) Surface decoration with gH625-membranotropic peptides as a method to escape the endo-lysosomal compartment and reduce nanoparticle toxicity. Nanotechnology 26:415101

Submit your manuscript to a SpringerOpen journal and benefit from:

- ► Convenient online submission
- ► Rigorous peer review
- ► Open access: articles freely available online
- ► High visibility within the field
- ► Retaining the copyright to your article

Submit your next manuscript at ► springeropen.com